Nano Research
https://doi.org/10.1007/s12274-017-1802-1
Research Article
ISSN 1998-0124
CN 11-5974/O4

Electric field and photoelectrical effect bi-enhanced hydrogen evolution reaction

Mengyu Yan[1,2,§], Xunbiao Zhou[1,§], Xuelei Pan[1], Junhui Wang[1], Lixue Xia[1], Kesong Yu[1], Xiaobin Liao[1], Xu Xu[1], Liang He[1], and Liqiang Mai[1] (✉)

[1] *State Key Laboratory of Advanced Technology for Materials Synthesis and Processing, International School of Materials Science and Engineering, Wuhan University of Technology, Wuhan 430070, China*
[2] *Materials Science and Engineering Department, University of Washington, Seattle, Washington 98195-2120, United States*
[§] *Mengyu Yan and Xunbiao Zhou contributed equally to this work.*

Received: 17 July 2017
Revised: 9 August 2017
Accepted: 12 August 2017

KEYWORDS
electrochemical,
device,
hydrogen evolution reaction,
photoelectrical effect,
field effect

ABSTRACT

Molybdenum disulfide (MoS_2) is an earth-abundant and low-cost hydrogen evolving electrocatalyst with the potential to replace traditional noble metal catalysts. The catalytic activity can be significantly enhanced after modification due to higher conductivity and enriched active sites. However, the underlying mechanism of the influence of the resistance of electrode material and contact resistance on the hydrogen evolution reaction (HER) process is unclear. Herein, we present a systematic study to understand the relationship between HER performance and electrode conductivity, which is bi-tuned through the electric field and photoelectrical effect. It was found that the onset overpotential consistently decreased with the increase of electrode conductivity. In addition, the reduction of the contact resistance resulted in a quicker electrochemical reaction process than enhancing the conductivity of the MoS_2 nanosheet. An onset overpotential of 89 mV was achieved under 60 mW/cm^2 sunlight illumination (0.6 sun) and a simultaneous gate voltage of 3 V. These physical strategies can also be applied to other catalysts, and offer new directions to improve HER catalytic performance of semiconductor materials.

1 Introduction

Hydrogen is a renewable and clean energy carrier which has attracted significant attention as a way to meet the increasing global energy demand and curb environmental pollution [1, 2]. Water, which consists of only hydrogen and oxygen, is an ideal source of hydrogen. Generating hydrogen through water splitting offers a non-polluting and cost-efficient route for the scalable production of hydrogen fuel. In this process, it is necessary to employ an economical and efficient catalyst [3, 4]. It is well known that Pt-group precious

Address correspondence to mlq518@whut.edu.cn

metals have excellent hydrogen evolution reaction (HER) performance, as they have an ultralow onset overpotential and facilitate fast reaction kinetics [5–7]. Nevertheless, the high cost of these catalysts limits their large-scale application [8]. In view of this limitation, the development of high-efficiency, high-stability, and earth-abundant electrocatalysts is urgently needed.

Molybdenum disulfide (MoS_2), one of the transition metal dichalcogenides (TMDs), has gained increasing interest for its unique crystal structure, optical, and electronic properties in recent years [9–14]. In addition, many experimental and theoretical studies have demonstrated that MoS_2 has an adequate Gibbs free energy of adsorbed atomic hydrogen, which is necessary for electrochemical water splitting [15]. However, poor conductivity and active sites only located at the edges of the material limit the HER performance of MoS_2. To achieve higher activity of MoS_2-based catalysts, great effort has been devoted to increasing the number of active sites or controlling the electron transport [16–21]. Recent studies have shown that the catalytic activity of MoS_2 could be improved by mechanically induced phase transformation from the stable 2H to the metastable 1T phase, accompanied by enhanced conductivity [22–25].

It is well known that both the field effect and photoelectrical effect can improve the conductivity of MoS_2 and other semiconductors by tuning the energy band and generating photo electrons, respectively [9, 11, 26]. The field effect can decrease the contact resistance and improve the conductivity of electrode material, while the photoelectric effect only improves the conductivity. Thus, attempts were made to understand the influence of contact and sheet resistances on the HER performance with MoS_2 as the catalyst. In this work, the electric field and photoelectrical effect were both tuned in fabricated electrocatalytic devices with individual MoS_2 nanosheets as the catalysts. We demonstrate that the onset overpotential constantly decreases with increasing electrode conductivity. In addition, a faster electrochemical reaction process was achieved by reducing the contact resistance. Finally, an overpotential of 89 mV was achieved at a current density of 10 mA/cm^2 under 60 mW/cm^2 sunlight illumination (0.6 sun) and a simultaneous gate voltage of 3 V.

2 Results and discussion

Figures 1(a) and 1(b) show the schematic and optical image of individual MoS_2 nanosheet-based HER device, respectively. The device integrates an electrochemical three-electrode system including a MoS_2 nanosheet (working electrode), a platinum wire (counter electrode) and a saturated calomel electrode (reference electrode). The fabrication procedure is schematically illustrated in Fig. S1 in the Electronic Supplementary Material (ESM). In this device, the MoS_2 nanosheets were obtained through a scotch-tape-based mechanical exfoliation method. The exfoliated MoS_2 consisted of a single-crystal structure, as shown in Fig. S2 in

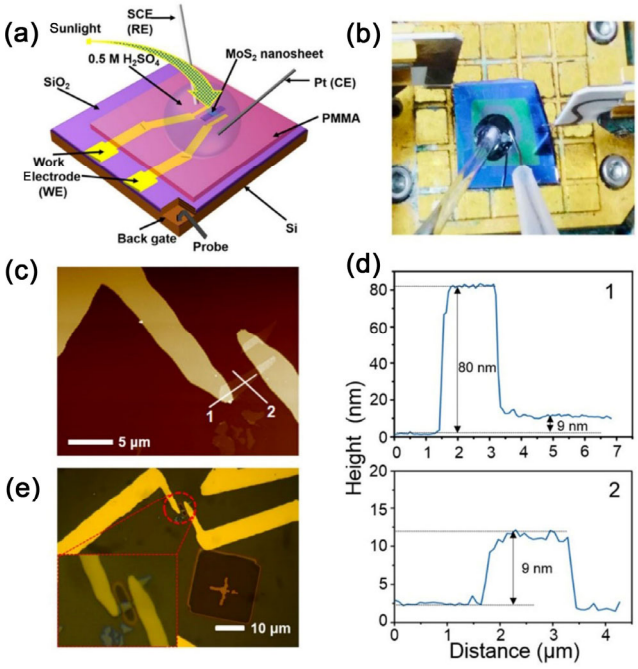

Figure 1 (a) Schematic of the individual MoS_2 nanosheet-based photo-electrochemical HER device with an incorporated microscopic electrochemical cell. 0.5 M H_2SO_4 was used as the electrolyte. In the device, the heavily doped silicon wafer (brown) was used as the back gate and a 300 nm thick SiO_2 layer (purple) was applied as the gate dielectric. This device enabled easy control of different back-gate voltages and illumination with a solar simulator. (b) Optical image of the individual MoS_2 nanosheet-based HER device assembled with counter and reference electrodes. (c) Optical micrograph of a typical MoS_2 nanosheet with two gold electrodes. (d) The height line profile drawn across the individual MoS_2 nanosheet and gold electrodes along white lines 1 and 2 in Fig. 1(c). (e) The optical image of the individual MoS_2 nanosheet device. The gold electrodes are protected by a PMMA-based insulating layer and a rectangular window is opened (inset image) between the gold electrodes to expose the MoS_2 nanosheet to the electrolyte.

the ESM. Then, MoS_2 nanosheets were selectively transferred to the Si/SiO_2 wafer. Two metal electrodes were then deposited on the individual MoS_2 nanosheet by using electron beam lithography (EBL) followed by Cr/Au (5 nm/65 nm) evaporation and a lift-off process (Fig. 1(c)). The thickness of the MoS_2 and Cr/Au electrode was measured using an atomic force microscope along the white lines 1 and 2, as shown in Fig. 1(c). The height line profiles drawn across the MoS_2 nanosheet and the Cr/Au electrode showed thicknesses of ~70 and 9 nm, respectively (Fig. 1(d)). Subsequently, the Cr/Au electrodes were protected by a polymethyl methacrylate (PMMA) layer and a window was left to expose the MoS_2 nanosheet (Fig. 1(e)). In this way, the electrochemical and electrical signal of the MoS_2 nanosheet was not influenced by the Cr/Au electrodes or the PMMA layer. The conductivity but the PMMA layer was shown to be much smaller than that of MoS_2 (Fig. S3 in the ESM). Thus, the actual signal of MoS_2 nanosheet can be obtained by this way. Finally, the exposed MoS_2 nanosheets were immersed in the electrolyte (0.5 M H_2SO_4), and integrated with a platinum wire and a saturated calomel electrode to form a three-electrode electrochemical system.

Based on the assembled individual nanosheet electrochemical device, the polarization curves of the blank sample, Au, MoS_2 nanosheet, and Pt were measured (Fig. 2(a)). There was only a small amount of HER activity observed for the blank sample, in which the Au electrodes were insulated by the PMMA layer and not in contact with any MoS_2 nanosheets (Fig. S4 in the ESM). The onset overpotential of Au was determined to be ~523 mV, which will not influence the onset overpotential of MoS_2 (379 mV). An excellent onset overpotential of 20 mV was achieved for Pt at a current density of 10 mA/cm^2 and the Tafel slope was found to be 40 mV/dec, which is consistent with results from conventional three-electrode systems [27]. Raman spectroscopy was used to investigate the influence of electrocatalytic processes, and the spectra can be seen in Fig. 2(b) [28–30]. No obvious Raman band shift occurred after the electrocatalytic test, which indicates that the structure of the MoS_2 was not changed. The influence of the heat from sunlight illumination was also investigated. The device was illuminated under a solar cell simulator with an irradiation intensity of 60 mW/cm^2 for over 3 min, and then the solar cell was turned off to test the polarization curve of MoS_2. It was found that the polarization curves of the MoS_2 nanosheets were similar for illuminated and non-illuminated samples after 185 s of simulated sunlight (Fig. 2(c)). This indicates that the temperature of the surface of the MoS_2 nanosheets does not change significantly with sunlight illumination.

The sunlight illumination and back-gate voltage were adjusted to tune the electrocatalytic performance of the individual MoS_2 nanosheet, in an attempt to understand the relationship between the conductivity of catalyst, contact resistance, and the electrocatalytic performance. It was found that the onset overpotential of the MoS_2 nanosheet decreases consistently from 379, 362, 276 to 259 mV by applying back-gate voltages of 0, 1, 2, and 3 V, respectively (Fig. 3(a) and Fig. S5(b) in the ESM). Interestingly, a large change of overpotentials is observed when MoS_2 nanosheets are exposed to the 60 mW/cm^2 sunlight illumination. The onset overpotential of the MoS_2 nanosheet changes to 254, 208, and 169 mV with sunlight illumination at back-gate voltages of 1, 2, and 3 V, respectively (Fig. 3(a) and

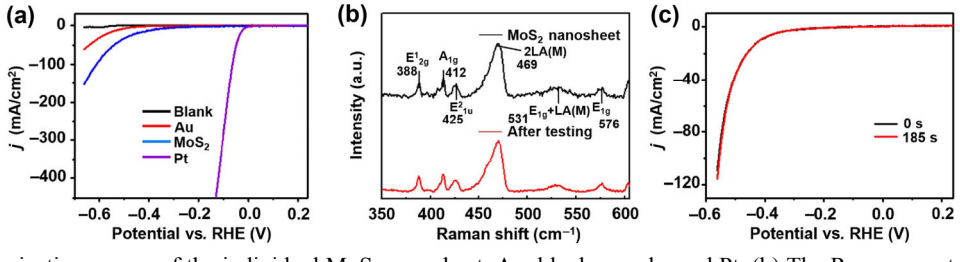

Figure 2 (a) Polarization curves of the individual MoS_2 nanosheet, Au, blank sample, and Pt. (b) The Raman spectra of the individual MoS_2 nanosheet before and after the photo-electrochemical test. (c) Polarization curves of the individual MoS_2 nanosheet before and after 185 s of sunlight illumination.

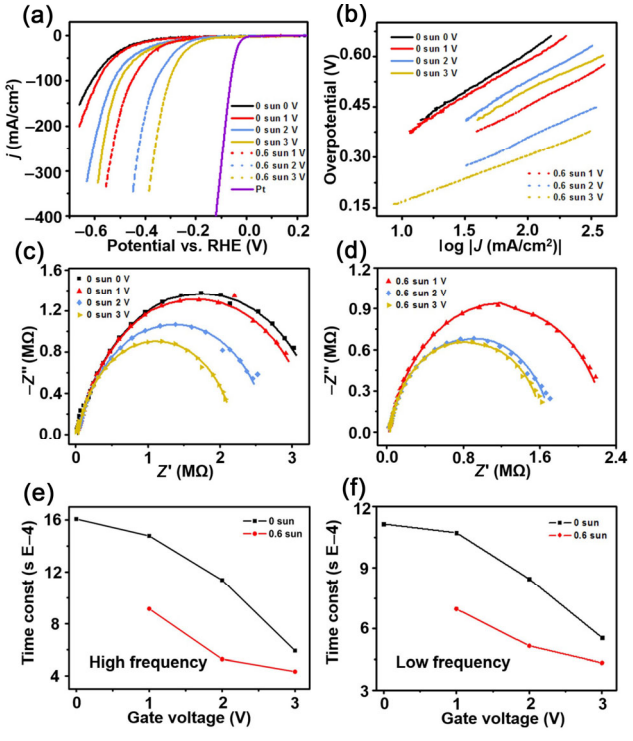

Figure 3 (a) Polarization curves and (b) corresponding Tafel plot of the individual MoS_2 nanosheet under gate voltages of 0–3 V and with/without irradiation at an intensity of 60 mW/cm^2. (c) and (d) Nyquist plot and plot of corresponding (e) high frequency time constant (τ_1) and (f) low frequency time constant (τ_2) of the individual MoS_2 nanosheet under gate voltages of 0–3 V and with/without irradiation at an intensity of 60 mW/cm^2.

Fig. S5(b) in the ESM). Similar trends are also observed in the Tafel plots, which were continuously optimized with increasing back-gate voltage and under sunlight illumination (Fig. 3(b) and Fig. S5(c) in the ESM). In addition, to determine the significance of the measured variations, we measured three other samples and obtained their onset overpotentials (Table S1 in the ESM). Coincident with increasing back-gate voltage and sunlight illumination, the onset overpotential of all the samples decreased dramatically (Fig. S5(a) in the ESM). The lowest onset overpotential of the four samples tested was 89 mV (at 10 mA/cm^2; Table S1). To investigate the mechanism of the effect of back-gate voltage and sunlight illumination on overpotential, electrochemical impedance spectra of the individual MoS_2 nanosheet was measured. The Nyquist plots are shown in Figs. 3(c) and 3(d). The Nyquist plots indicate a two-time constant model as two linked semicircles appear on the complex plane without a diffusion control step. The impedance spectra with different back-gate voltages and sunlight illumination was fitted to a modified Armstrong's equivalent circuit (Fig. S6(a) in the ESM). The plots of charge transfer resistance (R_{ct}) and electro-desorption/recombination reaction resistance (R_p) are shown in Figs. S6(b) and S6(c) in the ESM. The R_{ct} decreases continuously from 3.66 to 2.16 MΩ with increasing back-gate voltage from 0 to 3 V and further drops from 2.36 to 1.54 MΩ with 60 mW/cm^2 sunlight illumination. This drop indicates accelerated reactions kinetics, which is further demonstrated by the variety of R_p. Both the high (τ_1) and low frequency time constants (τ_2) decreased dramatically by adding a back-gate voltage and sunlight illumination (Figs. 3(e) and 3(f)). It was demonstrated that a much faster charge transfer process [31, 32], as well as the electro-desorption and/or recombination reactions, occurred while the MoS_2 nanosheet was tuned by back-gate voltage or under the sunlight illumination, which may benefit from the enhanced conductivity.

To further explain the results described above, the *I*–*V* characteristic measurement was performed on the MoS_2 nanosheets without electrolyte at different gate voltages and lighting intensities, as shown in Fig. 4(a) and its inset image. The potential window ranged from −0.5 to 0.5 V. The channel conductivity of the individual MoS_2 nanosheets increased from 3.48 to 24.02 S/m when increasing the back-gate voltage from 0 to 3 V. In addition, the conductance increased to 26.07, 37.82, and 49.22 S/m upon illumination with sunlight and applying varying the back-gate voltages between 1 and 3 V (Fig. S7 in the ESM). The electric field can reduce the contact resistance between the 2H MoS_2 nanosheet and the substrate, facilitating electron injection from the electrode to the active sites [33]. When sunlight illumination was applied to the 9 nm thick nanosheet, most of the photons can be absorbed by the MoS_2 layers and then photo electrons were generated [34]. These charge carriers migrate to the top layer by interlayer transport and are coupled to absorbed hydronium (H_3O^+) in the HER. Thus, both of these strategies have the potential to enhance electron transfer kinetics and accelerate the electrocatalytic production of hydrogen.

To investigate the influence of contact resistance

and sheet resistance on the catalytic process, the catalysis was measured at a gate voltage between 3 and 1 V combined with sunlight illumination, which resulted in similar electrode conductivities of 24.02 and 26.07 S/m, respectively. In thermodynamic system, the electrodes showed similar onset overpotentials of 259 and 254 mV. For the kinetics, the Tafel slope of the 3 V gate voltage was lower than the 1 V gate voltage combined with sunlight illumination. The comparison of τ_1 and R_{ct} (Fig. 3(e) and Fig. S6(b) in the ESM) supports our view that the 3 V gate voltage results in a faster electrochemical reaction by facilitating a faster charge transfer process. In other words, it is more effective to reduce the contact resistance with back-gate voltage than to enhance the MoS_2 sheet conductivity with sunlight illumination for increased reaction kinetics.

The chronoamperometry of the MoS_2 nanosheet was measured at a constant applied potential of −0.66 V vs. reversible hydrogen electrode (RHE) under various gate voltages between 0 and 3 V and with/without irradiation intensity of 60 mW/cm^2. It was found that the current density rised initially, and then remains relatively constant (Fig. 4(b)). Thus, both the illumination and back-gate voltage can improve the electrocatalysis performance by improving the conductivity of the MoS_2 nanosheet. The fluctuation at the beginning of the measurement does not influence the accuracy of the experimental results and shows that achieving a stable catalytic state requires a process for catalysts [35, 36]. To better understand the effect of sunlight illumination on the MoS_2 nanosheet, physical characterization was performed at a 5 mV voltage by applying two-second pulses of 60 mW/cm^2 sunlight illumination. Typical photoswitching behavior can be observed in Fig. 4(c) which demonstrates the excellent photosensitivity of the pristine MoS_2 thin films. Chronoamperometry measurement of the individual MoS_2 nanosheet was also performed to explore the correlation between electrochemical properties and sunlight illumination in a three-electrode configuration. The activity of the electrocatalyst had a strong and rapid response to illumination with sunlight (Fig. 4(d)). The catalytic current almost immediately increased by 50% or more and recovered to its original state when the solar simulator was turned off.

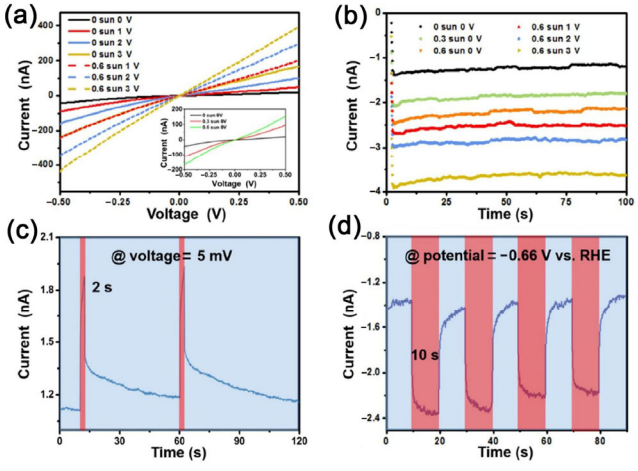

Figure 4 (a) The *I–V* curves of an individual MoS_2 nanosheet under gate voltages of 0 to 3 V and with/without irradiation at an intensity of 60 mW/cm^2. The inset image is the *I–V* curves of the individual MoS_2 nanosheet with irradiation intensities of 0, 30, and 60 mW/cm^2. (b) Chronoamperometry measurements of the MoS_2 nanosheet at a constant applied potential of −0.66 V vs. RHE under gate voltages of 0 to 3 V and with/without irradiation at an intensity of 60 mW/cm^2. (c) Sunlight illumination dependent chronoamperometry measurement of the MoS_2 nanosheet at a 5 mV voltage in the presence of electrolyte. Two-second pulses of sunlight illumination were applied at 10 and 60 s, which are highlighted with a red background. (d) Electrochemical potential dependent chronoamperometry measurement of the MoS_2 nanosheet at an overpotential of −0.66 V vs. RHE. Ten-second pulses of sunlight illumination were applied at 10, 30, 50, and 70 s, which are highlighted with red background.

The system fabricated in this study is used for electrocatalytic hydrogen production, with a 60 mW/cm^2 sunlight illumination applied to tune the electrochemical properties of MoS_2. Different from general photocatalysis, in which there are both light-harvesting materials as catalysts and active materials as cocatalysts, the thin flake of the MoS_2 serves as the active material and simultaneously generates electron–hole pairs via sunlight illumination in the electrochemical three-electrode system [34].

3 Conclusions

We have designed and fabricated a photo-electrochemical HER device based on individual MoS_2 nanosheet. Back-gate voltage and sunlight illumination were applied simultaneously to tune the catalytic performance of the MoS_2 nanosheets. With increasing gate

voltage from 0 to 3 V, the onset overpotential dropped from 379 to 259 mV and further to 169 mV when illuminated at an intensity of 60 mW/cm^2. The electrode conductivity was also continuously enhanced in this process. The R_{ct} decreased from 3.66 to 1.54 MΩ and the τ_1 dropped from 1.6 to 0.5 ms, which demonstrated an accelerating charge transfer process. By comparing the catalytic performance and conductivity at different gate voltages and sunlight illuminations, we demonstrated that facilitating electron injection from the electrode to the active sites can achieve faster charge transfer kinetics and hydrogen evolution rate than generating photo electrons in MoS_2 layers. This purely physical strategy to utilize electric field and photoelectrical effects simultaneously may lead to more environmentally friendly hydrogen production and provide a new direction for other important industrial reactions.

4 Experimental

4.1 Fabrication of the individual MoS_2 nanosheet photo-electrochemical device

A suitable-sized silicon substrate (with a 300 nm thick insulation layer) was ultrasonically cleaned and patterned outer electrodes (Cr/Au, 5 nm/50 nm) were formed by ultraviolet lithography and physical vapor deposition. Then, the MoS_2 nanosheets were obtained through a scotch-tape-based mechanical exfoliation method and were selectively transferred to the Si/SiO_2 wafer. Two metal inner electrodes were deposited on the MoS_2 nanosheets by using EBL followed by Cr/Au (5 nm/65 nm) evaporation and a lift-off process. Finally, spin-coating was performed to deposit a PMMA layer to protect the Cr/Au electrodes and a window was left to expose the MoS_2 nanosheet.

4.2 Material and device characterization

A Renishaw INVIA micro-Raman spectroscopy system was utilized to obtain the Raman spectra. XRD (Bruker D8 Advanced X-ray diffractometer with Cu-Kα radiation) was used to characterize the structural phases of the bulk MoS_2 sample. EBL was performed using a JEOL-7100F microscope and the atomic force microscopy image was obtained by scanning probe microscopy (Bruker MultiMode VIII). The electrochemical performances of the prepared devices were tested using an autolab 302N, probe station (Lake Shore, TTPX) and a semiconductor device analyzer (Agilent B1500A).

4.3 Electronic conductivity and electrochemical measurements

Both a probe station and semiconductor device analyzer were used to measure the electrical transport characteristics of the individual MoS_2 nanosheets. A three-electrode configuration was set up to measure the catalytic performance of the individual MoS_2 nanosheet-based photo-electrochemical HER device. In this configuration, the individual MoS_2 nanosheets served as the working electrode. A platinum wire electrode served as the counter electrode and a saturated calomel electrode was the reference electrode. The 0.5 M H_2SO_4 solution was used as the electrolyte. The polarization curve of the HER was obtained at a scan rate of 5 mV/s and electrochemical potential dependent chronoamperometry measurements were performed at a constant applied potential of −0.66 V vs. RHE using a solar simulator (Newport 94023A). All the electrochemical measurements were carried out using an autolab combined probe station, solar simulator, and semiconductor device analyzer.

Acknowledgements

This work was supported by the National Key Research and Development Program of China (Nos. 2016YFA0202603 and 2016YFA0202604), the National Basic Research Program of China (No. 2013CB934103), the National Natural Science Foundation of China (Nos. 51521001, 51272197, 51302203, 51502227, 51579198), the National Natural Science Fund for Distinguished Young Scholars (No. 51425204), the China Postdoctoral Science Foundation (No. 2015T80845), the Hubei Provincial Natural Science Fund for Distinguished Young Scholars (No. 2014CFA035), the Fundamental Research Funds for the Central Universities (WUT: 2014-IV-062, 2014-IV-147, 2016III001, 2016III005) and the National Students Innovation and Entrepreneurship

Training Program (WUT: 20161049701003). M. Y. Y. would like to acknowledge the support from State of Washington through the Washington Research Foundation Innovation Fellowship at the University of Washington Clean Energy Institute.

Electronic Supplementary Material: Supplementary material (the schematic diagram and optical image of the assembly process, XRD pattern of the exfoliated MoS_2, more *I*–*V* curves, the optical image of the blank sample, specific electrochemical data and corresponding variation tendency, and calculation details) is available in the online version of this article at https://doi.org/10.1007/s12274-017-1802-1.

References

[1] Dresselhaus, M. S.;Thomas, I. L. Alternative energy technologies. *Nature* **2001**, *414*, 332–337.

[2] Lewis, N. S.; Nocera, D. G. Powering the planet: Chemical challenges in solar energy utilization. *Proc. Natl. Acad. Sci. USA* **2006**, *103*, 15729–15735.

[3] Xu, X. M.; Chen, Y. B.; Zhou, W.; Zhu, Z. H.; Su, C.; Liu, M. L.; Shao, Z. P. A Perovskite electrocatalyst for efficient hydrogen evolution reaction. *Adv. Mater.* **2016**, 28, 6442–6448.

[4] Zou, X. X.; Zhang, Y. Noble metal-free hydrogen evolution catalysts for water splitting. *Chem. Soc. Rev.* **2015**, *44*, 5148–5180.

[5] Conway, B. E.; Jerkiewicz, G. Relation of energies and coverages of underpotential and overpotential deposited H at Pt and other metals to the "volcano curve" for cathodic H_2 evolution kinetics. *Electrochim. Acta* **2000**, *45*, 4075–4083.

[6] Esposito, D. V.; Hunt, S. T.; Kimmel, Y. C.; Chen, J. G. A new class of electrocatalysts for hydrogen production from water electrolysis: Metal monolayers supported on low-cost transition metal carbides. *J. Am. Chem. Soc.* **2012**, *134*, 3025–3033.

[7] Greeley, J.; Jaramillo, T. F.; Bonde, J.; Chorkendorff, I.; Nørskov, J. K. Computational high-throughput screening of electrocatalytic materials for hydrogen evolution. *Nat. Mater.* **2006**, *5*, 909–913.

[8] Stephens, I. E. L.; Chorkendorff, I. Minimizing the use of platinum in hydrogen-evolving electrodes. *Angew. Chem., Int. Ed.* **2011**, *50*, 1476–1477.

[9] Late, D. J.; Liu, B.; Ramakrishna Matte, H. S. S.; Dravid, V. P.; Rao, C. N. R. Hysteresis in single-layer MoS_2 field effect transistors. *ACS Nano* **2012**, *6*, 5635–5641.

[10] Baugher, B. W. H.; Churchill, H. O. H., Yang, Y. F.; Jarillo-Herrero, P. Intrinsic electronic transport properties of high quality monolayer and bilayer MoS_2. *Nano Lett.* **2013**, *13*, 4212–4216.

[11] Radisavljevic, B.; Radenovic, A.; Brivio, J.; Giacometti, V.; Kis, A. Single-layer MoS_2 transistors. *Nat. Nanotechnol.* **2011**, *6*, 147–150.

[12] Bao, W. Z.; Cai, X. H.; Kim, D.; Sridhara, K.; Fuhrer, M. S. High mobility ambipolar MoS_2 field-effect transistors: Substrate and dielectric effects. *Appl. Phy. Lett.* **2013**, *102*, 042104.

[13] Zhang, Y. J.; Ye, J. T.; Yomogida, Y.; Takenobu, T.; Iwasa, Y. Formation of a stable *p*−*n* Junction in a liquid-gated MoS_2 ambipolar transistor. *Nano Lett.* **2013**, *13*, 3023−3028.

[14] McDonnell, S.; Addou, R.; Buie, C.;Wallace, R. M.; Hinkle, C. L. Defect-dominated doping and contact resistance in MoS_2. *ACS Nano* **2014**, *8*, 2880–2888.

[15] Hinnemann, B.; Moses, P. G.; Bonde, J.; Jørgensen, P. K.; Nielsen, J. H.; Horch, S.; Chorkendorff, I.; Nørskov, J. K. Biomimetic hydrogen evolution: MoS_2 nanoparticles as catalyst for hydrogen evolution. *J. Am. Chem. Soc.* **2005**, *127*, 5308–5309.

[16] Gao, M. R.; Liang, J. X.; Zheng, Y. R.; Xu, Y. F.; Jiang, J.; Gao, Q.; Li, J.; Yu, S. H. An efficient molybdenum disulfide/cobalt diselenide hybrid catalyst for electrochemical hydrogen generation. *Nat. Commun.* **2015**, *6*, 5982.

[17] Merki, D.; Hu, X. L. Recent developments of molybdenum and tungsten sulfides as hydrogen evolution catalysts. *Energ. Environ. Sci.* **2011**, *4*, 3878–3888.

[18] Voiry, D.; Yang, J.; Chhowalla, M. Recent strategies for improving the catalytic activity of 2D TMD nanosheets toward the hydrogen evolution reaction. *Adv. Mater.* **2016**, *28*, 6197–6206.

[19] Wang, H. T.; Tsai, C.; Kong, D. S.; Chan, K. R.; Abild-Pedersen, F.; Nørskov, J. K.; Cui, Y. Transition-metal doped edge sites in vertically aligned MoS_2 catalysts for enhanced hydrogen evolution. *Nano Res.* **2015**, *8*, 566–575.

[20] Zhang, B.; Liu, J.; Wang, J. S.; Ruan, Y. J.; Ji, X.; Xu, K.; Chen, C.; Wan, H. Z.; Miao, L.; Jiang, J. J. Interface engineering: The $Ni(OH)_2/MoS_2$ heterostructure for highly efficient alkaline hydrogen evolution. *Nano Energy* **2017**, *37*, 74–80.

[21] Hu, W. H.; Shang, X.; Han, G. Q.; Dong, B.; Liu, Y. R.; Li, X.; Chai, Y. M.; Liu, Y. Q.; Liu, C. G. MoS_x supported graphene oxides with different degree of oxidation as efficient electrocatalysts for hydrogen evolution. *Carbon* **2016**, *100*, 236–242.

[22] Acerce, M.; Voiry, D.; Chhowalla, M. Metallic 1T phase MoS_2 nanosheets as supercapacitor electrode materials. *Nat. Nanotechnol.* **2015**, *10*, 313–318.

[23] Geng, X. M.; Sun, W. W.; Wu, W.; Chen, B.; Al-Hilo, A.; Benamara, M.; Zhu, H. L.; Watanabe, F.; Cui, J. B.; Chen, T. P. Pure and stable metallic phase molybdenum disulfide nanosheets for hydrogen evolution reaction. *Nat. Commun*. **2016**, *7*, 10672.

[24] Lin, Y. C.; Dumcenco, D. O.; Huang, Y. S.; Suenaga, K. Atomic mechanism of the semiconducting-to-metallic phase transition in single-layered MoS_2. *Nat. Nanotechnol.* **2014**, *9*, 391–396.

[25] Lukowski, M. A.; Daniel, A. S.; Meng, F.; Forticaux, A.; Li, L. S.; Jin, S. Enhanced hydrogen evolution catalysis from chemically exfoliated metallic MoS_2 nanosheets. *J. Am. Chem. Soc*. **2013**, *135*, 10274–10277.

[26] Yin, Z. Y.; Li, H.; Li, H.; Jiang, L.; Shi, Y. M.; Sun, Y. H.; Lu, G.; Zhang, Q.; Chen, X. D.; Zhang, H. Single-layer MoS_2 phototransistors. *ACS Nano* **2012**, *6*, 74–80.

[27] Thomas, J. G. N. Kinetics of electrolytic hydrogen evolution and the adsorption of hydrogen by metals. *Trans. Faraday Soc.* **1960**, *57*, 1603–1611.

[28] Gołasa, K.; Grzeszczyk, M.; Korona, K. P.; Bożek, R.; Binder, J.; Szczytko, J.; Wysmołek, A.; Babiński, A. Optical properties of molybdenum disulfide (MoS_2). *Acta Phy. Polonica A* **2013**, *124*, 849–851.

[29] Windom, B. C.; Sawyer, W. G.; Hahn, D. W. A Raman spectroscopic study of MoS_2 and MoO_3: Applications to tribological systems. *Tribol. Lett.* **2011**, *42*, 301–310.

[30] Zabinski, J. S.; Donley, M. S.; McDevittb, N. T. Mechanistic study of the synergism between Sb_2O_3 and MoS_2 lubricant systems using Raman spectroscopy. *Wear* **1993**, *165*, 103–108.

[31] Azizi, O.; Jafarian, M.; Gobal, F.; Heli, H.; Mahjani, M. G. The investigation of the kinetics and mechanism of hydrogen evolution reaction on tin. *Int. J. Hydrogen Energ.* **2007**, *32*, 1755–1761.

[32] Kibsgaard, J.; Jaramillo, T. F.; Besenbacher, F. Building an appropriate active-site motif into a hydrogen-evolution catalyst with thiomolybdate $[Mo_3S_{13}]^{2-}$ clusters. *Nat. Chem*. **2014**, *6*, 248–253.

[33] Voiry, D.; Fullon, R.; Yang, J.; de Carvalho Castroe Silva, C.; Kappera, R.; Bozkurt, I.; Kaplan, D.; Lagos, M. J.; Batson, P. E.; Gupta, G. et al. The role of electronic coupling between substrate and 2D MoS_2 nanosheets in electrocatalytic production of hydrogen. *Nat. Mater*. **2016**, *15*, 1003–1009.

[34] Velický, M.; Bissett, M. A.; Woods, C. R.; Toth, P. S.; Georgiou, T.; Kinloch, I. A.; Novoselov, K. S.; Dryfe, R. A.W. Photoelectrochemistry of pristine mono- and few-layer MoS_2. *Nano Lett*. **2016**, *16*, 2023–2032.

[35] Duan, J. J.; Chen, S.; Jaroniec, M.; Qiao, S. Z. Porous C_3N_4 nanolayers@N-graphene films as catalyst electrodes for highly efficient hydrogen evolution. *ACS Nano* **2015**, *9*, 931–940.

[36] Yan, M. Y.; Pan, X. L.; Wang, P. Y.; Chen, F.; He, L.; Jiang, G. P.; Wang, J. H.; Liu, J. Z.; Xu, X.; Liao, X. B. et al. Field-effect tuned adsorptiondynamics of VSe_2 nanosheets for enhanced hydrogen evolution reaction. *Nano Lett*. **2017**, *17*, 4109–4115.